CDK inhibitors p18^{INK4c} and p27^{Kip1} mediate two separate pathways to collaboratively suppress pituitary tumorigenesis

David S. Franklin,[1] Virginia L. Godfrey,[2] Hayyoung Lee,[3] Grigoriy I. Kovalev,[1,4] Robert Schoonhoven,[5] Selina Chen-Kiang,[3] Lishan Su,[1,4] and Yue Xiong[1,6,7,8]

[1]Lineberger Comprehensive Cancer Center, [2]Department of Pathology and Laboratory Medicine, [4]Department of Microbiology and Immunology, [5]Department of Environmental Sciences and Engineering, [6]Department of Biochemistry and Biophysics, and [7]Program in Molecular Biology and Biotechnology, School of Medicine, University of North Carolina at Chapel Hill, Chapel Hill, North Carolina 27599 USA; [3]Department of Pathology, Cornell University Medical College, New York, New York 10021 USA

INK4 and CIP/KIP are two distinct families of cyclin-dependent kinase (CDK) inhibitors implicated in mediating a wide range of cell growth control signals. We have created p18^{INK4c}-deficient mice. These mice develop gigantism and widespread organomegaly. The pituitary gland, spleen, and thymus are disproportionately enlarged and hyperplastic. T and B lymphocytes develop normally in p18-deficient mice, but both exhibit increased cellularity and a higher proliferative rate upon mitogenic stimulation. Loss of p18, like that of p27, but not other CDK inhibitor genes, leads to a gradual progression from intermediate lobe pituitary hyperplasia in young mice to an adenoma by 10 months of age with a nearly complete penetrance. Mice lacking both p18 and p27, like mice chimeric for Rb deficiency, invariably died from pituitary adenomas by 3 months. Hence, p18 and p27 mediate two separate pathways to collaboratively suppress pituitary tumorigenesis, likely by controlling the function of Rb.

[*Key Words*: CDK inhibitors; gene targeting; tumor suppression; growth regulation]

Received June 10, 1998; revised version accepted July 31, 1998.

To exert an effect on cell proliferation, most cell growth regulatory pathways must interact with the machinery that controls progression through the G_1 phase of the cell cycle. These pathways range from growth-activating events such as fertilization or mitogenic stimulation to growth-inhibitory signals like DNA damage, cell differentiation, or senescence. How these individual pathways interact at the molecular level with the G_1 cell cycle control pathway is largely unknown (Pardee 1989; Sherr 1994). The eukaryotic cell cycle is regulated primarily by a family of serine/threonine protein kinases, consisting of regulatory cyclin subunits and catalytic cyclin-dependent kinase (CDK) subunits (for review, see Hunter and Pines 1994; Morgan 1995). In mammalian cells, two CDK enzymes, CDK4 or CDK6 in combination with three D-type cyclins (D1, D2, and D3), and CDK2 in association with cyclin E, play distinct key roles in regulating G_1 progression. CDK4/6–cyclin D couple extracellular growth signals to the cell cycle, while CDK2–cyclin E controls the initiation of DNA replication (Sherr 1994). In contrast to the role of cyclins in mediating mitogenic stimulatory signals, CDK inhibitors are responsible for integrating many growth-inhibitory pathways. The expression of CDK inhibitor genes has been found to be induced by or correlated with a wide range of growth-inhibitory signals, such as mitogen starvation, cell–cell contact inhibition, DNA damage, antiproliferative cytokine treatment, terminal differentiation, and senescence, implicating CDK inhibitors in coupling diverse cell signaling pathways to the cell cycle machinery (Sherr and Roberts 1995).

The seven mammalian CDK inhibitor genes identified thus far belong to two separate families. The *INK4* family includes four closely related ankyrin repeat containing genes: p16^{INK4a}, p15^{INK4b}, p18^{INK4c}, and p19^{INK4d}, and the CIP1/KIP1 family contains three genes: p21$^{CIP1/WAF1}$, p27^{KIP1}, and p57^{KIP2} (Sherr and Roberts 1995). INK4 proteins selectively form binary complexes with CDK4 or CDK6 to prevent the CDKs from binding with and becoming activated by D-type cyclins. p21/p27/p57 inhibitors broadly regulate multiple CDK enzymes, including CDK4/6–cyclin Ds, by forming ternary complexes with CDK and cyclin pro-

[8]**Corresponding author.**
E-MAIL yxiong@email.unc.edu; FAX (919) 966-8799.

teins. These features make CDK4 and CDK6 unique among the members of the CDK family as the only CDKs regulated by both CIP/KIP and INK4 families of inhibitors, and broaden the ability of CDK4 and CDK6 to serve as integrators for the convergence of many growth control signaling pathways.

While the biochemical mechanism(s) by which CDK inhibitors regulate CDK activity is relatively well understood, most functional studies on CDK inhibitors were carried out in cultured cells and are largely correlative. To address this issue, a genetic approach has been taken to determine the function of CDK inhibitors by gene targeting. Despite common CDK targets shared by both families of CDK inhibitor proteins, no obvious phenotypic similarities have been observed thus far for any of the four CDK inhibitor genes that have been genetically disrupted. Mice lacking p21 are defective in a DNA-damage mediated G_1 checkpoint, but are developmentally normal and do not develop spontaneous tumors (Deng et al. 1995). Disruption of p16 (and its colocalized $p19^{ARF}$) results in the development of spontaneous tumors at an early age in numerous cell types (Serrano et al. 1996). Mice lacking p57 die soon after birth, displaying severe developmental defects with a varying degree of penetrance and phenotype similar to human patients with Beckwith–Wiedemann syndrome (Zhang et al. 1997; Yan et al. 1997). Disruption of p27 in mice results in a series of additional novel phenotypes including increased body size, multiorgan hyperplasia, female sterility, retinal dysplasia, and pituitary tumors (Fero et al. 1996; Kiyokawa et al. 1996; Nakayama et al. 1996). These effects argue a diverse range of functions for the different CDK inhibitor genes.

We previously isolated a member of the INK4 gene family, $p18^{INK4c}$, and showed that, like p16, ectopic expression of p18 in cultured cells suppresses cell growth with correlated dependence on endogenous wild-type pRB (Guan et al. 1994). The *p18* gene is widely expressed during mouse embryogenesis and accumulates to high levels in a number of terminally differentiated tissues and during cell aging (Guan et al. 1994; Franklin and Xiong 1996; Zindy et al. 1997; Phelps and Xiong 1998). Here, we report that mice lacking p18 exhibit a series of phenotypes remarkably similar to those seen in mice lacking p27, including development of widespread organomegaly, pituitary hyperplasia and adenoma, and a hyperproliferative response to mitogenic stimulation. The progression of pituitary tumors in mice lacking both p18 and p27 is greatly accelerated compared with either single gene disruption, indicating a functional collaboration between these two CDK inhibitors.

Results

Targeted deletion of the mouse p18 *gene*

We disrupted the mouse p18-coding region by homologous recombination (Fig. 1A; Material and Methods). The mouse *p18* gene contains three exons: exon 1 corresponding exclusively to the 5′-untranslated region and two coding exons, exons 2 and 3 (Phelps et al. 1998). The majority (75%) of the p18-coding region is contained in exon 3 (amino acid residues 42–168), and was targeted for deletion. In the targeting construct, a 2-kb *Eco*RI genomic fragment containing exon 3 was replaced with a neo^r cassette (Fig. 1A). After electroporation and selection of neomycin-resistant foci, two heterozygous $p18^{+/-}$ ES clones (C5 and C55) were identified by Southern blotting. Both ES clones were karyotyped normal and microinjected into C57BL/6 blastocysts to generate germ-line chimeras. Three male F_1 chimeras derived from ES clone C55 successfully mated with B6D2/F1J females to produce F_2 heterozygote offspring harboring the mutant INK4c allele. The F_2 heterozygotes were mated to produce the F_3 founder $p18^{+/+}$, $p18^{+/-}$ and $p18^{-/-}$ strains. All genotypes were verified by Southern blotting (Fig. 1B) and confirmed further by examination of the expression of p18 protein (Fig. 1C). No obvious difference in the level of p18 protein was detected between wild-type and heterozygous animals. Deletion of exon 3 generates a mutant INK4c allele that retains a small portion of p18 coding for the amino-terminal 41 residues of the p18 protein. The p18 antibody we used was raised against a carboxyl terminus peptide, preventing us from firmly excluding the possibility that the remaining 41 residues are expressed or could still bind to and interfere with the function of CDK4 and CDK6. However, this possibility seems very unlikely as deletion of the fourth ankyrin repeat in p16 (residue 110, corresponding to residue 102 at the carboxyl terminus in p18) completely abolished binding of p16 with CDK4 (Yang et al. 1995). Also, missense mutations of several residues in the third ankyrin repeat of p18 (e.g., Arg-79 and Asp-100), which are deleted in our p18-deficient mice, completely abolished binding of p18 and its inhibitory activity toward CDK4/CDK6 (S. Noh, Y. Li, Y. Xiong, and K.-L. Guan, unpubl.).

p18-null mice have increased body size and exhibit organomegaly

Mating of p18 heterozygous mice produced wild-type, heterozygous, and null pups in essentially the anticipated Mendelian ratio (18:32:17), indicating that p18 heterozygous and null embryos are viable. p18-null mice undergo normal development well into adulthood. Except for the pituitary tumor described below, we did not detect any increased rate of tumorigenesis in p18-null mice ranging from 1 to 13 months ($n = 30$), indicating that in most tissues, p18 alone may have only a limited or redundant role in tumor suppression. While previous studies correlated induced p18 expression and association with CDK4 and CDK6 during in vitro myogenesis and adipogenesis (Franklin and Xiong 1996; Phelps and Xiong 1998), we did not detect abnormal muscle or adipose development in p18-null animals, This indicates that p18 does not have an essential role in causing cell cycle withdrawal during the differentiation of these two tissues. Whether p18 plays a role in maintaining the cell cycle arrest in mature myotubes or adipocytes remains to be determined. Both male and female $p18^{-/-}$ animals

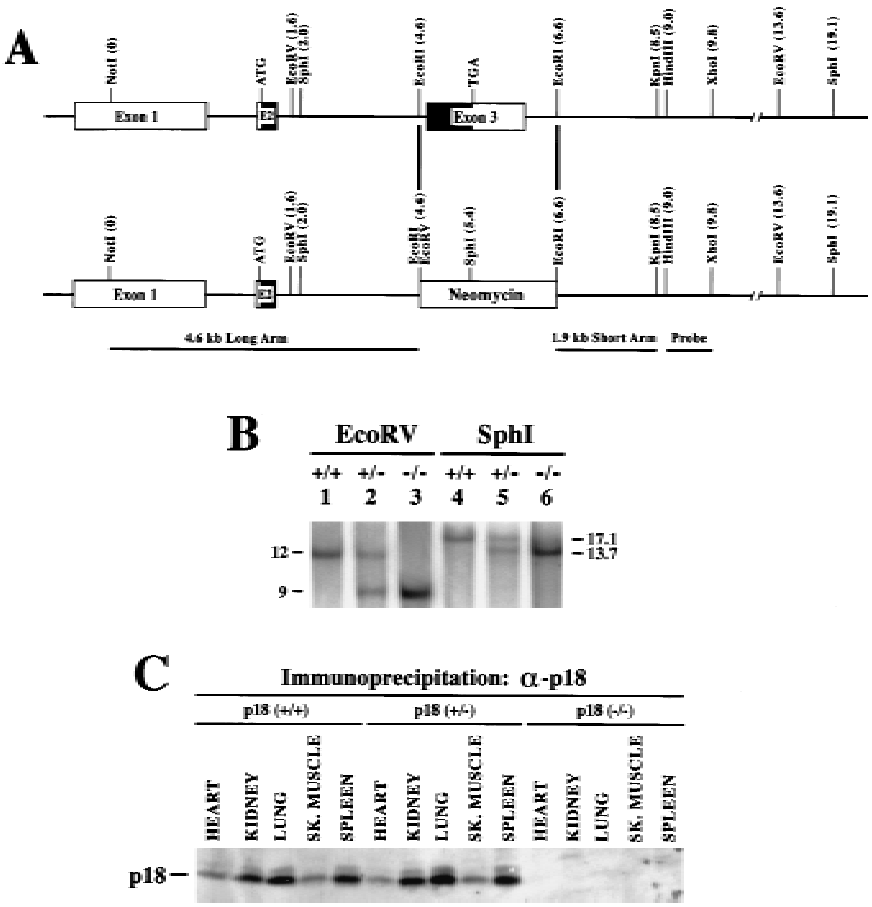

Figure 1. Targeted disruption of *p18*^{INK4c} locus. (*A*) Genomic structure of the mouse *INK4c* locus. The mouse *INK4c* locus contains three exons. Coding region is shown by black boxes. The relative positions of restriction sites and translation initiation and termination codons are indicated. *p18* was disrupted by replacement of the 2-kb *Eco*RI fragment containing exon 3 with the neo^r selectable marker. The 4.6- and 1.9-kb genomic fragments used for homologous recombination and the probe fragment used for Southern analysis are indicated. (*B*) Southern blot analysis of the *p18* locus. Genomic DNA from p18$^{+/+}$ (lanes *1*,*4*), p18$^{+/-}$ (lanes *2*,*5*) and p18$^{-/-}$ (lanes *3*,*6*) mice was digested with restriction enzymes *Eco*RV (lanes *1–3*) or *Sph*I (lanes *4–6*) and hybridized with a *p18* probe (see *A*). Molecular size markers are indicated. (*C*) p18 protein expression in mouse tissues. Total cell lysates were prepared from several p18$^{+/+}$, p18$^{+/-}$, and p18$^{-/-}$ tissues. Expression of p18 protein was determined by IP–Western blot analysis with antibodies specific for p18. The p18 protein is indicated.

are fertile and can mate successfully with wild-type or null animals. Litter number (88 litters for p18$^{+/+}$ and 81 litters for p18$^{-/-}$, $P = 0.336$) and size (8.9 pups/litter for p18$^{+/+}$ and 9.1 pups/litter for p18$^{-/-}$, $P = 0.672$) produced from these different matings are similar, indicating that lack of p18 function does not significantly impair reproduction.

At birth, wild-type, heterozygous, and null mice appear indistinguishable. However, within 2–3 weeks, the p18$^{-/-}$ mice became distinctly larger than their p18$^{+/+}$ littermates (Fig. 2A). A detailed analysis of this phenotype showed that as early as 9 days, p18$^{-/-}$ mice were 7.4% bigger than p18$^{+/+}$ littermates and 35%–45% larger by the end of 1 month (Fig. 2B). By day 33, even the smallest p18$^{-/-}$ female was bigger than the largest p18$^{+/+}$ male (Fig. 2C). We examined p18$^{-/-}$ mice externally and internally to determine whether any organs were disproportionately large with respect to their increased body size. Externally, p18$^{-/-}$ mice did not show any abnormal proportions. Internally, p18-deficient mice display widespread organomegaly (Fig. 2D). We compared the relative increase in body and organ weights between the p18-null and wild-type mice at 1, 2, and 3 months (Fig. 2E). Three organs, the heart, kidney, and liver, from null animals were roughly proportionate in weight to the increase in total body weight. However, the spleen and thymus were disproportionately enlarged. The body weight of null mice increased by 20%, 40%, and 30% at 1, 2, and 3 months, respectively. The weight of the spleen in p18-null animals increased disproportionately by 40%, 110%, and 90% during the same time points. The increase of thymus weight, twice the body weight increase in p18-null animals at 1 month, became proportionate to the body weight increase at 2 months, and was disproportionately small at 3 months. These observations suggest that loss of p18 function not only promotes disproportionate thymus growth at an early age, but also accelerates later thymic involution. Although larger than wild-type testes (Fig. 2D,E), the testes of 1-, 2-, and 3-month-old p18-null males were disproportionately small with respect to the body size (Fig. 2E). Two other organs that were difficult to weigh but showed apparent disproportionate enlargement were the adrenal (Fig. 2D) and the pituitary (see Fig. 4, below) glands.

There was no obvious difference in the levels of p18 protein between p18$^{+/+}$ and p18$^{+/-}$ tissues (Fig. 1C). Consistently, we did not observed any significant difference in the body and organ size between p18$^{+/+}$ and p18$^{+/-}$ mice (data not shown), indicating that there is no gene dose dependence for the p18 protein expression. This is different from loss of p27 function, where p27$^{+/-}$ heterozygotes were intermediate in size between small p27$^{+/+}$ and large p27$^{-/-}$ homozygotes. This suggests that in vivo p18 but not p27 protein levels are in excess for its function.

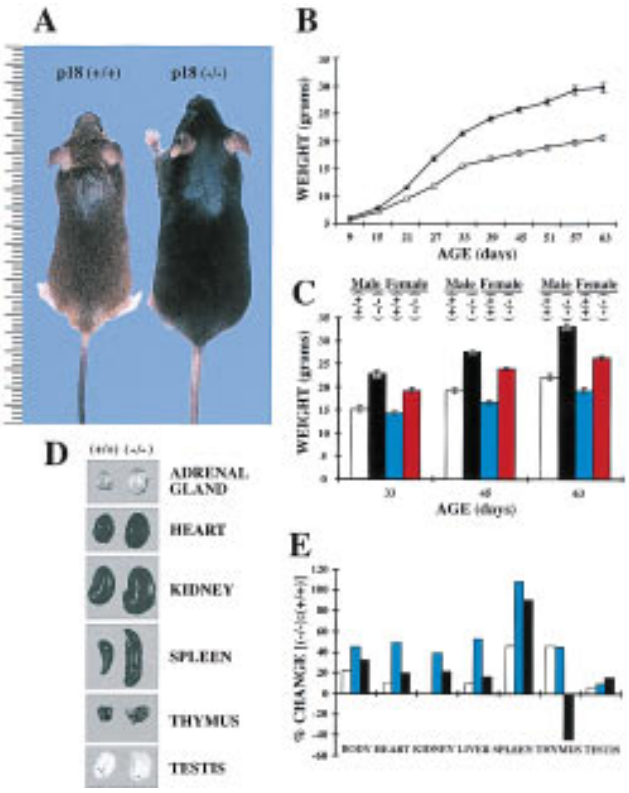

Figure 2. p18-deficient mice exhibit body size increase and organomegaly. (*A*) Wild-type (agouti, *left*) and p18-deficient (black, *right*) mice at 4 weeks of age. Size is indicated in centimeters. (*B*) Growth curve of p18-deficient (■) and wild-type (□) mice. Both genotypes (nine each) were weighed from age 9 to 63 days. Standard error bars are indicated. (*C*) Body weight comparison of male and female p18-deficient and wild-type mice. Data were taken from *B* for days 33, 45, and 63 and replotted according to gender: wild-type males (open bars), null males (black bars), wild-type females (blue bars), and null females (red bars). (*D*) Organomegaly in $p18^{-/-}$ mice. Gross appearance of adrenal gland, heart, kidney, spleen, thymus, and testis are shown for $p18^{+/+}$ and $p18^{-/-}$ animals. (*E*) Increase of body and individual organ weights in $p18^{-/-}$ mice relative to wild-type littermates. $p18^{+/+}$ and $p18^{-/-}$ animals were weighed at ages 1 month (open bars), 2 months (blue bars) and 3 months (black bars). Heart, kidney, liver, spleen, thymus, and testis from these mice were isolated and weighed. The data are plotted as relative body and individual organ weight differences of the $p18^{-/-}$ animal compared with the $p18^{+/+}$ animals.

Because the p18-null mice develop evident pituitary pathology (see below), which could produce an elevated level of growth hormones, an increase in body and organ size could result from endocrine abnormalities, rather than a defect in cell cycle control. For example, transgenic expression of growth hormone (GH; Palmiter et al. 1982), or insulin-like growth factor I (IGF-I; Mathews et al. 1988) results in a similar gigantism phenotype. GH or IGF-I transgenic mice, however, display certain histopathologies not detected in p18-deficient mice including hepatic hypertrophy, glomerular sclerosis, diffuse kidney tubular atrophy, and dermal abnormalities (Quaife et al. 1989). This observation argues against elevated growth hormones as a possible mechanism for gigantism in p18-deficient mice. Mice lacking p18 had normal serum level of GH (133 ng/ml GH for $p18^{+/+}$ and 62 ng/ml GH for $p18^{-/-}$, $P = 0.09$) and an only slight increase of IGF-I (516 ng/ml IGF-I for $p18^{+/+}$ and 739 ng/ml IGF-I for $p18^{-/-}$, $P = 0.11$). Therefore, we believe that the gigantism and organomegaly phenotypes resulted from an alteration in cell cycle control resulting from the loss of p18 function rather than endocrine effects. These observations, however, do not exclude the possibility that p18 functions downstream of the growth hormones in certain cell types.

p18-null mice display expansion of T lymphocytes and are hyper-responsive to mitogenic stimulation

Disproportionate enlargement of the thymus and spleen in young p18-null animals prompted us to examine hematolymphoid organs from wild-type and p18-null mice. FACS analysis showed a normal $CD4^+$ and $CD8^+$ T cell distribution in the thymus, lymph nodes (Fig. 3A), and spleen (data not shown) in p18-null animals, indicating normal T-lymphocyte development in the absence of p18. However, p18-null animals had a 40% increased thymic cellularity (Fig. 3B). A decrease in apoptosis does not seem to contribute significantly to the thymic hypercellularity, as apoptosis of thymocytes in response to CD3 stimulation was normal (data not shown) and was only slightly decreased in response to dexamethasone (31% in wild-type and 26% in p18-null thymocytes, $P = 0.06$, Fig. 3C).

To determine the effect of loss of p18 on T-lymphocyte proliferative response to mitogenic stimulation, we activated lymph node cells in vitro with concanavalin A (ConA). Cells were then pulse labeled with [^{3}H]thymidine, and DNA synthesis was determined (Fig. 3D). ConA-stimulated p18-null lymph node cells incorporated 3.1-fold more ^{3}H than the wild-type cells. We further evaluated the response of lymph node cells to ConA stimulation in vivo. Twelve hours after intraperitoneal ConA injection, lymph node cells were isolated and immediately pulse labeled with [^{3}H]thymidine. Consistent with the in vitro stimulation, in vivo mitogen-stimulated p18-deficient lymph node cells incorporated 3.3-fold more ^{3}H than stimulated wild-type lymph node cells (Fig. 3D).

To provide a mechanistic explanation for the increase of p18-null T-lymphocyte proliferation in response to mitogenic activation, we determined the CDK4 and CDK6 kinase activity of lymph node cells following mitogenic stimulation. Mice were injected with ConA, and lymph nodes were harvested 12 hr later. CDK4 and CDK6 immunocomplexes from lymph nodes of both wild-type and p18-null animals were assayed for their Rb kinase activity. While CDK4 immunocomplexes from both wild-type and p18-null lymphocytes contained similar levels of Rb kinase activity, CDK6 immunocomplexes from ConA-stimulated p18-null lymphocytes exhibited a 2.5-fold higher Rb kinase activity than those from wild-type cells (Fig. 3E). This result is consistent

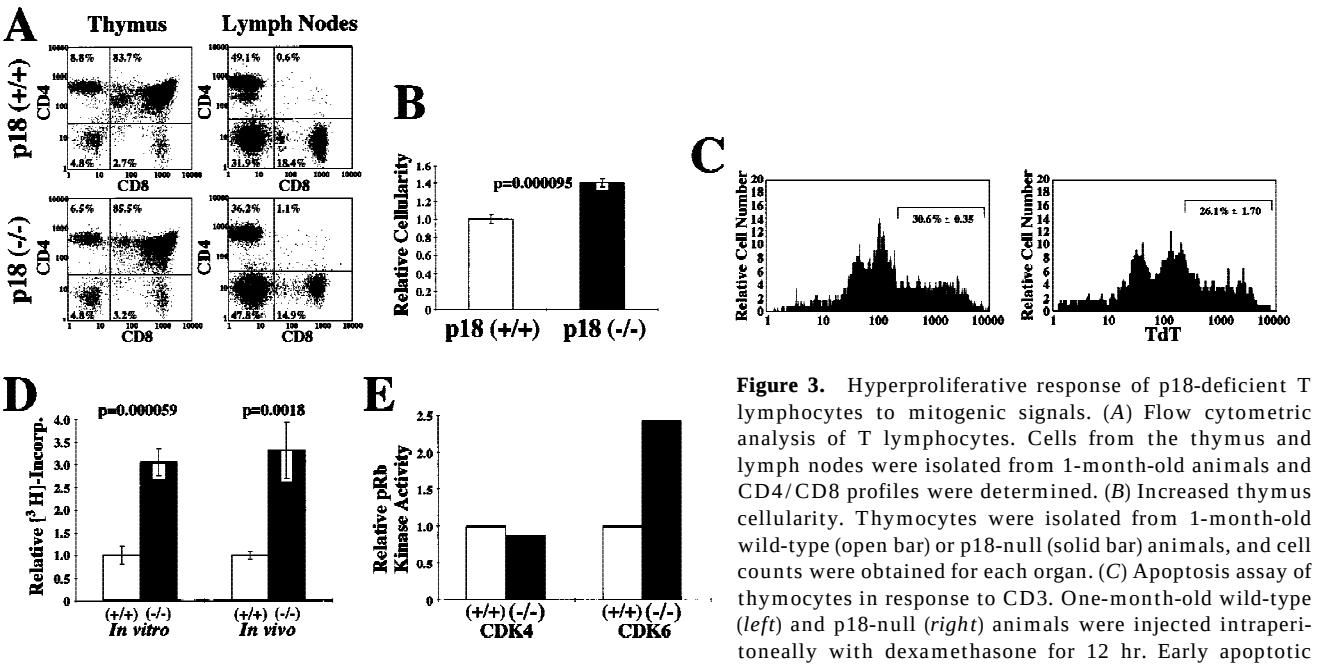

Figure 3. Hyperproliferative response of p18-deficient T lymphocytes to mitogenic signals. (*A*) Flow cytometric analysis of T lymphocytes. Cells from the thymus and lymph nodes were isolated from 1-month-old animals and CD4/CD8 profiles were determined. (*B*) Increased thymus cellularity. Thymocytes were isolated from 1-month-old wild-type (open bar) or p18-null (solid bar) animals, and cell counts were obtained for each organ. (*C*) Apoptosis assay of thymocytes in response to CD3. One-month-old wild-type (*left*) and p18-null (*right*) animals were injected intraperitoneally with dexamethasone for 12 hr. Early apoptotic cells were assayed by TdT end labeling and TdT–FITC FACS analysis. The percentage of apoptotic cells is indicated with standard error. (*D*) In vitro and in vivo proliferation of lymph node cells. For the in vitro assay, lymph node cells were isolated from 1-month-old wild-type (open bar) or p18-null (solid bar) animals and cultured in vitro. After ConA mitogenic stimulation, cells were pulsed with [^{3}H]thymidine. For in vivo stimulation, wild-type (open bar) and p18-null (solid bar) animals were injected intraperitoneally with ConA for 12 hr. Cells were isolated from lymph nodes and immediately pulsed with [^{3}H]thymidine. S-phase populations were determined by measurement of ^{3}H incorporation. (*E*) CDK4 and CDK6 kinase assay. Twelve hours after in vivo intraperitoneal ConA injection, CDK4 and CDK6 complexes were immunoprecipitated from wild-type (open bars) or p18$^{-/-}$ (solid bars) lymph nodes and assayed for their kinase activity with a GST–Rb fusion protein as substrate.

with the previous finding that p18 is preferentially associated with CDK6 compared with CDK4 (Guan et al. 1994) and that CDK6 is more prominently expressed than CDK4 in T lymphocytes (Meyerson and Harlow 1994). Increased CDK6 activity resulting from the loss of p18 function may provide a plausible molecular mechanism for the increased T-lymphocyte proliferation in response to mitogenic activation and the thymic hypercellularity seen in p18-null animals.

p18 negatively regulates cell cycle entry of resting B lymphocytes

Enlargement of the spleen in p18-null animals led us to examine B-lymphocyte development and their T-dependent response. B cells from the spleen and bone marrow of p18-null mice showed normal B220 and IgM distributions, indicating that B-cell development, like that of T cells, was normal in the absence of p18 function (Fig. 4A). At 2 months, p18-null animals had increased cellularity in both the spleen and bone marrow (Fig. 4B). To determine the molecular mechanism underlying the hypercellularity in the spleen, we purified resting B lymphocytes from the spleens of wild-type or p18-null mice and stimulated them in vitro with CD40 ligand (CD40L) and IL-6 (see Material and Methods). The number of activated, viable IgM$^+$ B cells began to increase after 3 days of treatment, and there was a 30% increase of p18-deficient B cells over wild-type B cells (Fig. 4C). The increased expansion of activated B cells in p18-null animals, both in vivo and in vitro, may have resulted from an increase of cell proliferation or decrease of apoptosis as B-cell activation is dynamically balanced by apoptosis in the germinal centers. The percentage of cells undergoing apoptosis, following treatment with either CD40L alone or CD40L together with IL-6, was comparable in p18-null and wild-type B cells (Fig. 4D), indicating that a decrease in apoptosis does not contribute significantly to splenic hypercellularity. The increase in activated B lymphocytes in the absence of p18 was therefore a consequence of an increase in proliferation rate.

CD40 signaling alone can stimulate resting B cells to enter the cell cycle. IL-6, although by itself does not possess mitogenic activity, can enhance the mitogenic stimulatory effect of CD40L. Unexpectedly, stimulation of p18-deficient resting B cells with CD40L alone, in the absence of IL-6, resulted in a 2.5-fold increase in the number of activated, viable IgM$^+$ B cells over that of wild-type cells, nearly approaching the proliferative rate of wild-type resting B cells stimulated by both CD40L and IL-6 (Fig. 4C). These results suggest that p18 has a role in limiting the expansion of B-cell clones in vivo in T-dependent humoral immune response and that a function for IL-6 in helping stimulate resting B cells with CD40L may be to antagonize the inhibitory activity of p18.

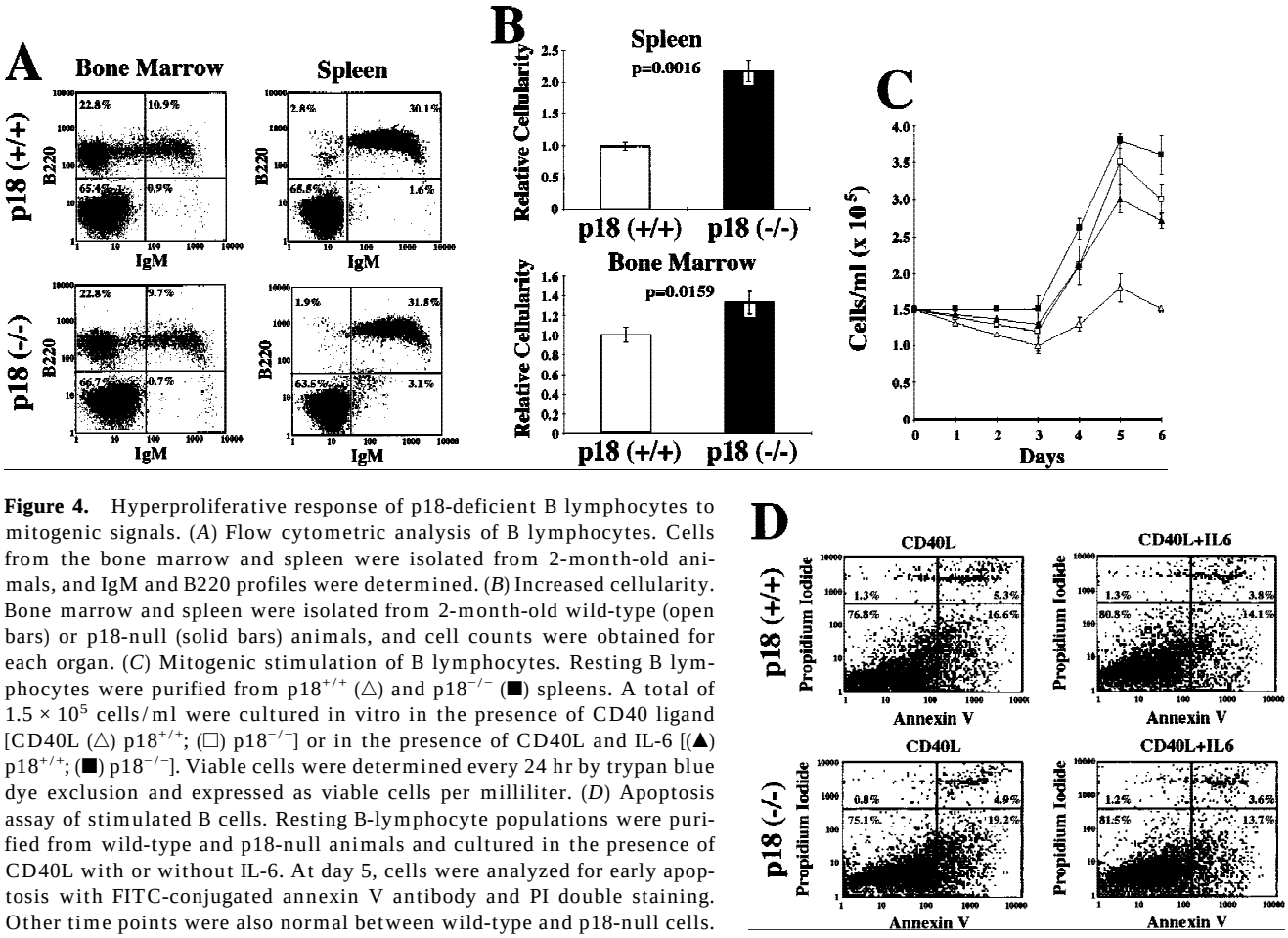

Figure 4. Hyperproliferative response of p18-deficient B lymphocytes to mitogenic signals. (*A*) Flow cytometric analysis of B lymphocytes. Cells from the bone marrow and spleen were isolated from 2-month-old animals, and IgM and B220 profiles were determined. (*B*) Increased cellularity. Bone marrow and spleen were isolated from 2-month-old wild-type (open bars) or p18-null (solid bars) animals, and cell counts were obtained for each organ. (*C*) Mitogenic stimulation of B lymphocytes. Resting B lymphocytes were purified from $p18^{+/+}$ (△) and $p18^{-/-}$ (■) spleens. A total of 1.5×10^5 cells/ml were cultured in vitro in the presence of CD40 ligand [CD40L (△) $p18^{+/+}$; (□) $p18^{-/-}$] or in the presence of CD40L and IL-6 [(▲) $p18^{+/+}$; (■) $p18^{-/-}$]. Viable cells were determined every 24 hr by trypan blue dye exclusion and expressed as viable cells per milliliter. (*D*) Apoptosis assay of stimulated B cells. Resting B-lymphocyte populations were purified from wild-type and p18-null animals and cultured in the presence of CD40L with or without IL-6. At day 5, cells were analyzed for early apoptosis with FITC-conjugated annexin V antibody and PI double staining. Other time points were also normal between wild-type and p18-null cells.

Progression of pituitary hyperplasia to adenoma in mice lacking p18

In 15 of 15 examined $p18^{-/-}$ mice ranging from 4 weeks to 13 months, the pituitary glands were enlarged compared with those of $p18^{+/+}$ control mice and displayed a pattern of hyperplastic or neoplastic progression. Hyperplasia in the intermediate and anterior pituitary lobes could be detected microscopically as early as 4 weeks in $p18^{-/-}$ mice. As the p18-null mice aged, we detected increasing hyperplasia in these lobes. Mild hyperplasia was detected in 1- to 3-month-old $p18^{-/-}$ mice ($n = 6$), moderate hyperplasia was detected in 4- to 8-month-old mice ($n = 5$), and severe hyperplasia or an intermediate lobe adenoma was found in 9- to 13-month-old mice ($n = 4$, see below). Slight compression of the neurohypophysis by the enlarged adenohypophysis was first detected at 5 and 6 months of age and compression became more pronounced in 9- to 13-month-old $p18^{-/-}$ mice. Histologic examination of a healthy looking 10-month-old $p18^{-/-}$ mouse revealed severe intermediate lobe hyperplasia (Fig. 5D,E). The anterior lobe was also enlarged in this $p18^{-/-}$ mouse, but not to the same degree as the intermediate lobe. No abnormal structures, such as atypical cells, cystic structures, increased vascularity, or interstitial hemorrhages, were detected in the pituitary of this mouse, (data not shown).

PCNA staining of pituitary gland tissue in juvenile animals (<6 weeks) was similar between $p18^{+/+}$ and $p18^{-/-}$. Pituitary sections from a 6-week-old p18-null animals showed minor increases in PCNA staining compared with age-matched controls. In young $p18^{-/-}$ adults (4–8 months), the pituitary was moderately enlarged and reflected only minor increases in PCNA staining. However, in older animals (9–13 months), the pituitary was greatly enlarged and was associated with a more pronounced PCNA staining, particularly in animals that develop intermediate lobe adenomas (see below).

Three of four 10-month-old or older $p18^{-/-}$ mice that we followed were visibly ataxic, thin, and dehydrated. Histologic examination of all three debilitated animals revealed a large pituitary adenoma (Fig. 5G). The adenomas originated from the intermediate lobe (Fig. 5H) and the cells stained strongly for adrenocorticotropic hormone (ACTH; Fig. 5I). These adenomas severely compressed, but did not invade the adjacent anterior lobe, though the neurohypophysis was always obliterated. A hyperplastic nodule was also noted adjacent to one of the adenomas and may have derived from the anterior lobe. The intermediate lobe tumor and hyperplastic nodule

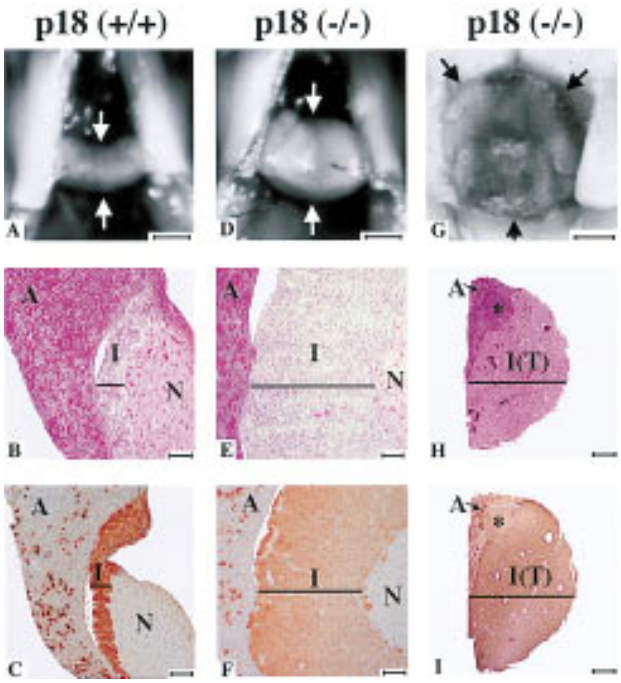

Figure 5. Pituitary tumorigenesis in $p18^{-/-}$ mice. Pituitaries from $p18^{+/+}$ (healthy 10-month-old, *A–C*), $p18^{-/-}$ (healthy 10-month-old with hyperplasia, *D–F*) and $p18^{-/-}$ (debilitated 9.5-month-old with adenoma, *G–I*). (*A*,*D*,*G*) Comparative sizes of pituitaries. Arrows indicate pituitaries. Bar, 1 mm. (*B*,*E*,*H*) Histological staining of the pituitaries. Cross sections of pituitaries of $p18^{+/+}$ (*B*) and $p18^{-/-}$ (*E*) and mid-sagittal section of $p18^{-/-}$ mice (*H*) were stained with hematoxylin and eosin. (A) Anterior lobe; (I) intermediate lobe; [I(T)] intermediate lobe tumor; and (N) neurohypophysis. (*) Hyperplastic nodule. (Black bars) Width of the intermediate lobe. Size bars, ~70 µm for *B* and *E* and 1 mm for *H*. (*C*,*F*,*I*) ACTH staining of pituitaries. Cross-section of pituitaries of control $p18^{+/+}$ (*C*) and $p18^{-/-}$ (*F*) and mid-sagittal section of $p18^{-/-}$ mice (I) were stained for ACTH. Abbreviations and symbols are as in other panels. Size bars, ~70 µm for *C* and *F* and 1 mm for *I*.

stained moderately for PCNA. These results indicate a slow, age-dependent progression of the pituitary phenotype in p18-null mice: from mild intermediate lobe hyperplasia to moderate and severe hyperplasia associated with increasing PCNA staining, compression of adjacent lobes, and finally the development of an intermediate lobe adenoma.

We compared pituitary ACTH expression in wild-type and null animals by immunohistochemistry (Fig. 5C,F). Immunostaining revealed uniform ACTH expression in the intermediate lobe of $p18^{-/-}$ and $p18^{+/+}$ mice. Plasma levels of ACTH have not been determined. Because the intermediate lobe of $p18^{-/-}$ mice is enlarged, it might be postulated that an increase in serum ACTH levels could contribute to the enlargement of the adrenal gland (Fig. 2D), specifically the adrenal cortex. However, there was no histological evidence of adrenal cortical hyperplasia (data not shown).

Loss of p18 function does not affect the level of p27 and p27–CDK complexes

There are striking phenotypic similarities between mice lacking p18 and those lacking p27 (Fero et al. 1996; Kiyokawa et al. 1996; Nakayama et al. 1996). Both mice are developmentally normal, but display increased body size, widespread organomegaly, multiple organ hyperplasia, increased lymphocyte mitogenic responses and develop spontaneous intermediate lobe pituitary lesions with 100% penetrance. Two different mechanisms may account for such phenotypic similarities. Either p18 and p27 function on the same pathway in a upstream–downstream manner, and loss of one may lead to a decreased expression or function of the other. Alternatively, p18 and p27 mediate two separate pathways, but converge on common targets.

To distinguish these two mechanisms, we examined the level of p27 expression and its complex formation with the three G_1 CDKs (CDK2, CDK4, and CDK6) in p18-deficient cells. We chose the spleen and thymus for this analysis as they are associated with hyperproliferative phenotypes in both p18- and p27-null animals. Total protein lysates were prepared from both tissues from wild-type and p18-null animals and analyzed for their expression of CDK2, CDK4, and CDK6 as well as the association of these CDKs with p27. The steady-state levels of all three CDK proteins were not changed by the loss of p18 in both tissues (Fig. 6A) as well as in several other tissues that we examined (e.g., testis, data not shown). The level of p27 protein was not changed by the loss of p18 function, nor was its association with CDK2, CDK4, and CDK6 (Fig. 6B).

p18 and p27 collaboratively suppress pituitary tumor growth

Analysis of p27 expression and its association with the CDK proteins indicated that p18 and p27 are unlikely to act on the same pathway. To conclusively determine the mechanism underlying the phenotypic similarities between p18- and p27-deficient mice, we generated mice lacking both genes by crossing p18-null mice to mice carrying a disruptive mutation in the cyclin–CDK inhibition domain of p27 (Kiyokawa et al. 1996). Mating of $p18^{+/-}$; $p27^{+/+}$ mice with $p18^{+/+}$; $p27^{+/-}$ mice produced all four genotypes in an essentially 1:1:1:1 Mendelian ratio (4:5:6:4, respectively). Mating between the mice heterozygous for both genes similarly produced all genotypes with anticipated Mendelian ratios, indicating that embryos with partial or complete loss of both p18 and p27 function are viable. Mutations of both p18 and p27 genes in the double-mutant mice were determined by Southern blotting (Fig. 6C) and verified further by examination of the expression of both proteins in pituitary tissues (Fig. 6D).

Consistent with previous reports (Nakayama et al. 1996; Kiyokawa et al. 1996; Fero et al. 1996) and similar to the phenotype seen in p18 mutant mice, in 20 p27-null mice that we have examined between the ages of 1

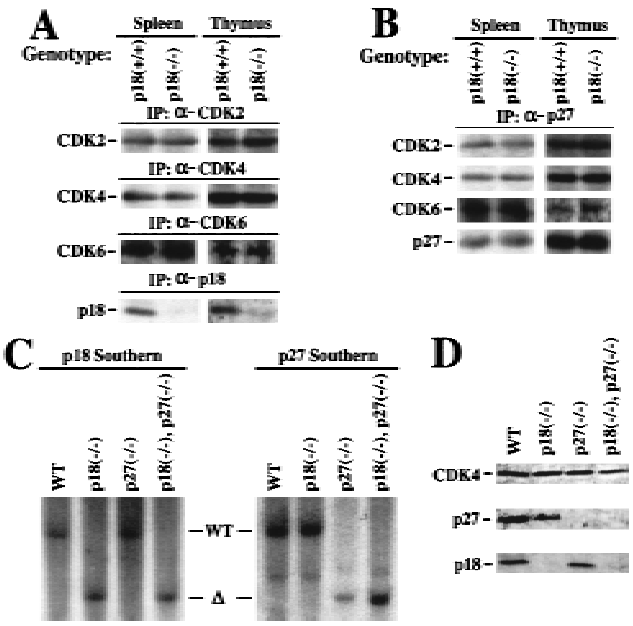

Figure 6. p27 and p27–CDK complexes in p18-deficient mice. (*A*) Expression of G1 CDK2, CDK4, and CDK6 is unchanged in p18-null cells. Total protein lysates were prepared from thymuses and spleens of wild-type or p18-null mice. The levels of the three CDK and p18 proteins were determined by IP–Western blot analysis with the indicated antisera. (*B*) p27–CDK complexes were not affected in p18-null cells. Total protein lysates prepared from thymuses and spleens of wild-type or p18-null mice were precipitated with anti-p27 antibody, and the level of p27 associated CDK proteins was determined by immunoblotting. (*C*) Generation of $p18^{-/-}/p27^{-/-}$ double-mutant mice. Southern blot analysis of the p18 and p27 loci. Genomic DNA from mice with four different genotypes was digested with *Eco*RV (for p18) or *Eco*RI (for p27) and hybridized with a p18 and a p27 probe as indicated. (*D*) Expression of p18 and p27 proteins in mice pituitary. Equal amounts of total cell lysates prepared from pituitary tissues of mice with four different genotypes were resolved by SDS-PAGE. p18 and p27 protein levels were determined by immunoblotting. The level of CDK4 protein remains relatively constant in different genetic backgrounds and was used as an additional control.

and 11 months, pituitary tumors were detected only in the two oldest animals (8 and 11 months, respectively), and not in the other 18 younger animals. Not a single p27 mutant mouse died of a pituitary tumor. Mice lacking both p18 and p27 functions initially appeared to be developmentally normal. By three months they appear visibly thin, ataxic, and dehydrated. All p18/p27 double-deficient mice died by 3.5 months of pituitary tumors ($n = 17$). In addition to the accelerated rate of pituitary tumorigenesis, many organs, such as the spleen, thymus, heart, testis, and adrenal gland, were more enlarged in the p18/p27 double-null mice than in either p18- or p27-deficient mice (data not shown). These observations provide genetic evidence that simultaneous loss of both p18 and p27 exaggerated the phenotype caused by the deficiency of either single gene, indicating that these two genes function in separate pathways to collaboratively regulate cell growth. Because the pituitary tumorigenesis represents a well-characterized phenotype and can be compared quantitatively by the rate of tumor progression, we focused our study on determining p18/p27 interaction on pituitary tumor development. A detailed characterization of the p18/p27 double-null mice will be described elsewhere.

We examined the pituitaries from 1- and 3-month-old wild-type, $p18^{-/-}$, $p27^{-/-}$, or $p18^{-/-}/p27^{-/-}$ animals. Pituitaries from either p18- or p27-null animals at the same age were comparable in size and were always larger than age-matched wild-type controls (Fig. 7A). In addition, both possessed hyperplastic intermediate lobes larger than wild-type animals (Fig. 7B). The histological appearance of the pituitary gland of $p18^{-/-}/p27^{-/-}$ double-null animals was evidently different from either single-null animal at the same age. The pituitaries from 1-month-old $p18^{-/-}/p27^{-/-}$ animals were greatly enlarged, and the intermediate lobe was more hyperplastic than that of either single-null animal. The intermediate lobe already stained moderately for PCNA, and the neurohypophysis was slightly compressed. By 3 months, $p18^{-/-}/p27^{-/-}$ animals developed pituitary tumors comparable to 10-month-old p18-null or p27-null animals. No $p18^{-/-}/p27^{-/-}$ animal survived past 3.5 months—all

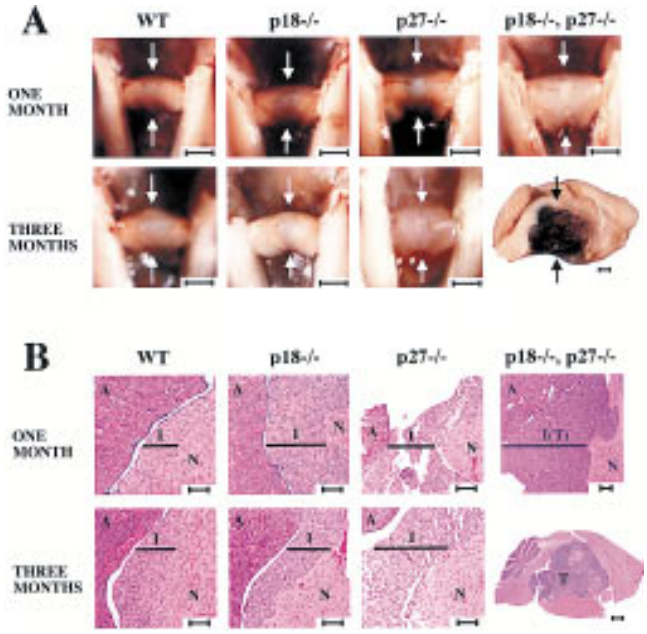

Figure 7. Pituitary tumorigenesis in $p18^{-/-}/p27^{-/-}$ mice. (*A*) Pituitaries from wild-type, $p18^{-/-}$, $p27^{-/-}$, and $p18^{-/-}/p27^{-/-}$ mice at 1 and 3 months were compared. (Arrows) Pituitaries. Bars, 1 mm. Note the different size bar (also 1 mm) for the pituitary from the 3-month-old $p18^{-/-}/p27^{-/-}$ mouse. (*B*) Histological staining of wild-type, $p18^{-/-}$, $p27^{-/-}$, and $p18^{-/-}/p27^{-/-}$ pituitaries. Cross sections or mid-sagittal sections of pituitaries of the four different genotypes were stained with hematoxylin and eosin. (*A*) Anterior lobe; (I) intermediate lobe; and (N) neurohypophysis. (Black bars) Width of the intermediate lobe. Size bars, 70 mm, except for the pituitary from the 3-month-old $p18^{-/-}/p27^{-/-}$ mouse (1 mm).

dying from pituitary adenomas. On the basis of invasion into the adjacent nerves, one of the $p18^{-/-}/p27^{-/-}$ animals was diagnosed with a pituitary carcinoma. This synergistic response in p18/p27 double-null animals provides genetic evidence that p18 and p27 functionally collaborate to suppress pituitary tumor growth.

Discussion

Function of p18 in growth control

Mice lacking p18 develop gigantism and widespread organomegaly, indicating a broad role of p18 in the growth control of many different cell types. Consistent with this notion is the observation that the *p18* gene is expressed widely in multiple tissues (Fig. 1C, and Guan et al. 1994; Franklin and Xiong 1996; Zindy et al. 1997; Phelps and Xiong 1998). Despite widespread hyperplasia and organomegaly, loss of p18 function does not cause gross congenital defects and all organs displaying hyperplasia (e.g., the thymus and spleen) appear developmentally normal. These observations indicate that p18 is not required for cell viability and organomorphogenesis and that p18 does not have an essential role in causing the cell cycle withdrawal during terminal cell differentiation. Withdrawal of mitogenic stimuli during terminal differentiation still enables cell cycle arrest in p18-deficient cells as in wild-type cells. Only when cells are challenged by mitogenic stimuli, can the effect of p18 loss on cell growth become evident. Cell cycle arrest brought about during terminal cell differentiation is apparently dominant over deregulated cell proliferation caused by the loss of the growth-suppressive activity of p18.

Increase in organ size can be caused by either an increase in cell number (hyperplasia), increase in individual cell size (hypertrophy) or a decrease in apoptosis. Examination of p18-deficient mice did not reveal any cell type with abnormal hypertrophy. In both T lymphocytes and splenic B cells, there was no obvious decrease in apoptosis (Figs. 4,5). Instead, in both the spleen and thymus, the increase in the organ size correlated with an increase in cell number. The mechanism underlying this increase in the cell number caused by the loss of p18 function is not clear at present. It is conceivable that loss of p18 function may shorten the G_1 interval, leading to a faster cell division cycle in precursor or progenitor cells, thereby contributing to an increase in cell number prior to the cell cycle withdrawal during terminal cell differentiation.

Function of p18 in lymphocyte mitogenic activation

Optimal T- or B-cell activation requires stimulation from at least two signals, such as CD3 and CD28 (or IL-2) for T cells, or B-cell receptor (or IL-6) and CD40L for B cells. CD40-activated B cells enter the cell cycle and can be stimulated further by addition of cytokines (for a recent review, see Van Kooten and Banchereau 1997). The mechanism underlying the requirements for these two signals is unknown. IL-6 is a pleiotropic cytokine that can enhance the mitogenic activity of CD40L in stimulating resting B cells to enter the cell cycle (Fig. 4). The proliferation rate of p18-deficient B cells in response to CD40L stimulation in the absence of IL-6 is similar to that of wild-type B cells in response to co-stimulation by CD40L and IL-6 (Fig. 4C). This finding provides genetic evidence suggesting a role for p18 in negatively regulating G_1 progression of B lymphocytes in response to CD40L and a function for IL-6 in antagonizing the inhibitory activity of p18 in resting B-cell activation. We further speculate that one function of the CD40 signaling pathway is to activate cyclin D expression. Such thinking would be consistent with the observation that CD40 alone (after prolonged stimulation), but not IL-6, is able to induce resting B cells into the cell cycle. Induction of cyclin D can eventually titrate off the p18-imposed block, but down-regulation of p18 in the absence of D cyclins is apparently not sufficient to activate CDK4/6. In principle, this mechanism can be utilized in other mitogenic events such as T cell activation that also requires two signaling pathways to achieve full activation.

p18 and p27 mediate two separate pathways and collaborate functionally

Among the many phenotypic similarities shared between p18- and p27-deficient mice, perhaps the most striking is the development of pituitary tumors. Not only are the tumors in both mice of the same intermediate lobe origin, but they also progress at essentially the same rate, succumbing to pituitary adenoma by ~10–12 months. The function of both genes in suppressing pituitary tumorigenesis is consistent with the observation that both p18 and p27 proteins are highly expressed in the pituitary tissues (Fig. 6D). The specificity of this function is further underscored by the fact that mice deficient for three other CDK inhibitor genes, *p16* (Serrano et al. 1996), *p21* (Deng et al. 1995), and *p57* (Zhang et al. 1997; Yan et al. 1997) do not develop pituitary anomalies.

Significantly, pituitary tumorigenesis in mice lacking both *p18* and *p27* genes is greatly accelerated. Pituitary adenomas can be detected histologically by 1 month and all $p18^{-/-}/p27^{-/-}$ mice die of pituitary tumors by 3.5 months (Fig. 6). This observed synergy provides the first genetic evidence for a specific functional collaboration between two CDK inhibitors. We have also crossed p18-null mice with mice carrying a disrupted p21 CDK inhibitor gene (Deng et al. 1995). Unlike mice deficient for both p18 and p27, mice lacking both *p18* and *p21* genes do not develop pituitary tumors at any faster rate than the mice lacking the *p18* gene alone (D. Franklin and Y. Xiong, unpubl.), further confirming and emphasizing the specificity of functional collaboration between p18 and p27. The biochemical mechanism underlying the functional collaboration between p18 and p27 is not known at present. Cooperation between CDK inhibitors has been observed previously during antimitogenic cytokine TGF-β-induced G_1 cell cycle arrest (Reynisdottir et al.

1995; Reynisdottir and Massague 1997). p15, induced by TGF-β, binds to CDK4/6, which coincides with a decrease (release) of CDK4/6-bound (sequestered) p27 and an increase of CDK2–p27 association. These observations led to an interpretation that p15 and p27 function in an upstream–downstream fashion on a single pathway in which p15 acts genetically as a regulator of p27. During in vitro-induced myogenesis and adipogenesis, p18 is significantly induced, yet, there is no detectable change in the levels of p27–CDK2, p27–CDK4, and p27–CDK6 complexes (Franklin and Xiong 1996; Phelps and Xiong 1998). In this study, we compared the level of p27 and its association with CDK2, CDK4, and CDK6 between wild-type and p18-deficient cells from several tissues that developed the overgrowth phenotype in the absence of p18 and did not detect any obvious changes in p27–CDK complexes (Fig. 6). Therefore, both genetic and biochemical evidence argues against the possibility that p18 acts as an upstream regulator of p27 in a linear fashion. Rather, these two genes appear to mediate two separate pathways, and retaining both pathways is necessary to completely suppress pituitary tumor growth (Fig. 8).

The only other gene whose loss of function resulted in pituitary tumor formation is the retinoblastoma gene, *Rb* (Jacks et al. 1992; Lee et al. 1992; Hu et al. 1994; Robanus Maandag et al. 1994; Williams et al. 1994). The biochemical functions of both p18 and p27 in inhibiting CDK activity and the cell cycle-dependent phosphorylation of Rb by CDKs leads us to suggest further that Rb is the common target of both p18- and p27-mediated tumor suppression pathways in the pituitary (Fig. 8). Supporting this notion is the observation that growth suppression by p18, like p16, correlates with the wild-type Rb function (Guan et al. 1994). Both the average age of pituitary tumor manifestation (~8–10 months) and its near complete penetrance in heterozygous Rb mice are intriguingly similar to those of p18 or p27 single-mutant mice (Hu et al. 1994). The rate of pituitary tumorigenesis is greatly accelerated in Rb chimeras, most of which succumb to pituitary tumors at ~4 months (Williams et al. 1994; Robanus Maandag et al. 1994), and is almost the same as in $p18^{-/-}/p27^{-/-}$ mice.

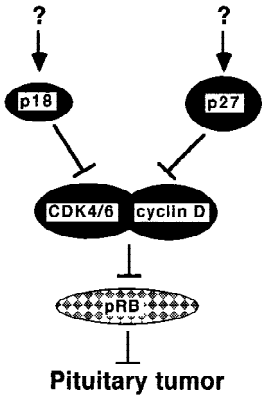

Figure 8. Suppression of pituitary tumorigenesis by p18 and p27. p18 and p27 mediate two separate pathways to collaboratively suppress pituitary tumorigenesis. The upstream regulatory signals leading to the activation of p18 and p27 are unknown. Rb is suggested to be the common target of p18 and p27 function on the basis of the observations that the biochemical functions of p18 and p27 are to inhibit CDK activity regulating pRb function and that chimeric $Rb^{-/-}$ mice and $p18^{-/-}/p27^{-/-}$ double-deficient mice develop pituitary tumors at essentially the same rate.

Of the four *INK4* CDK inhibitor genes, only $p16^{INK4a}$ has been linked directly to tumor suppression despite its product sharing almost indistinguishable biochemical properties with the other three INK4 proteins. Frequent genetic alteration of *p16* and its three downstream genes—*cyclin D1*, *CDK4/6*, and *Rb*—and the nonoverlapping pattern of their mutations in different types of human cancer has led to the hypothesis that *p16–CDK4/cyclin D1–Rb* pathway may function as a common genetic target in oncogenic transformation (Serrano et al. 1996; Sherr 1996). Notably, however, mice lacking p16 (and exon 2 of $p19^{ARF}$), while developing spontaneous tumors at multiple sites and at an early age, do not display any pituitary abnormality (Serrano et al. 1996). Together with the observation that p18/p27 double-null mice develop pituitary tumors at the same rate as Rb chimeric mice, we conclude that, at least in the mouse, it is not p16, but p18 and p27 that play the major role in suppressing tumorigenesis in certain tissues by controlling the function of Rb.

Material and methods

Gene targeting and generation of null mice

A 19-kb murine $p18^{INK4c}$ genomic clone was isolated from a 129/Sv mouse genomic λFIXII library (Stratagene, La Jolla, CA) by screening with a mouse *p18* cDNA probe (Phelps et al. 1998). The genomic clone was mapped by restriction digest analysis and partially sequenced. A deletion targeting plasmid, p18KO, derived from the pPNT vector (Tybulewicz et al. 1991), was constructed by use of two p18 genomic fragments: a 4.6-kb *Not*I–*Eco*RI and a 1.9-kb *Eco*RI–*Kpn*I fragment. These fragments flank a 2-kb *Eco*RI fragment containing *p18* exon 3 (see Fig. 1A, and Phelps et al. 1998). The resulting p18KO targeting vector was electroporated into 129/Sv embryonic stem (ES) cells. Fifty independent G418-resistant colonies were analyzed for p18 status by Southern blot analysis with *Eco*RV-digested genomic DNA hybridized with a 0.8-kb probe, which detects an ~12-kb fragment in the wild-type allele and a 9-kb fragment in the targeted mutant allele. Targeted ES clones were verified further with the same probe hybridized to *Sph*I-digested genomic DNA generating an ~14-kb fragment in the wild-type allele and a 17-kb fragment in the targeted mutant allele. Two $p18^{+/-}$ ES clones that karyotyped normal were microinjected into C57BL/6 blastocysts and implanted into foster B6 females. Eleven resulting F_1 male chimeras were backcrossed to B6D2 females. Three of the chimeras, all derived from one of the ES clones, transmitted agouti coat color via their germ line. Several F_2 heterozygotes were identified by Southern blot analysis and mated to produce F_3 wild-type, heterozygous, and p18-null littermates, which were used as founders. Intercrosses have been carried out to F_6 and F_7 without any alteration of the observed phenotypes. The p27-null mice were derived from CJ7 p27 heterozygous ES cells also microinjected into C57BL/6 blastocysts as described previously (Kiyokawa et al. 1996). Chimeric F_1 p27

males were backcrossed with C57BL/6 females to produce F_2 p27 heterozygotes. The p18/p27 double-null mice were derived from crossing p18-null F3 mice with $p27^{+/-}$ mice. Mice were genotyped, and the resulting F_2 p18/p27 double heterozygotes were intercrossed to create the double-null animal. Therefore, all four genotypes (wild type, p18 null, p27 null and p18/p27 double null) were mostly B6 in their genetic background. All genotypes were confirmed by Southern blot and verified by immunoblotting with antibodies specific to p18 or p27 proteins (Figs. 1,6).

Anatomic and histologic analysis

To measure body weights, 18 (9 males and 9 females) wild-type or p18-null mice were weighed every 6 days. Organs were isolated and weighed from 1-, 2-, and 3-month old wild-type or p18-null mice (three males and three females for each genotype and time point). For histological analysis, tissues were fixed in 10% buffered formalin, dehydrated by use of increasing concentrations of ethanol, cleared in xylene, and embedded in paraffin. Slides prepared with 5-µm sections were stained with hematoxylin and eosin.

Antibodies and immunochemistry

Antisera for p18, p27, CDK2, CDK4, and CDK6 (Xiong et al. 1993; Franklin and Xiong 1996), immunoprecipitations (IP), and immunoblotting procedures have been described previously (Jenkins and Xiong 1995). Protein lysate concentrations were determined by Bradford assay and equalized for each experiment. Kinase assays were performed as described previously (Franklin and Xiong 1996; Phelps and Xiong 1997). PCNA immunohistochemistry was performed on formaldehyde-fixed pituitary sections from age-matched wild-type, p18-null, or p18/p27 double-null mice. Hydrated tissue sections were rinsed in PBS containing 1% Tween-20 (PBS-T). Hydrogen peroxide quenching, PBS-T washes, staining with primary (mouse anti-human PC10 antibody, 1:100 dilution, Dako Corp., Carpinteria, CA) and secondary (goat anti-mouse IgG antibody, undiluted, Dako Corp.) antisera, visualization by the chromogen 3′3′-diaminobenzidine (DAB) and counterstaining with hematoxylin were performed according to methods provided in the Dako Envision Kit (Dako Corp.). ACTH immunostaining was performed on formaldehyde-fixed pituitary sections from 10-month-old wild-type and p18-null mice. Hydrated tissue sections were rinsed in PBS and quenched 10 min in 3% hydrogen peroxide solution in 100% methanol. Antigen retrieval was enhanced by heating sections in a microwave to 96°C for 8 min in a citric acid buffer (1.8 mM citric acid, 8.2 mM sodium citrate). Sections were blocked with 2% normal goat serum, stained with primary (rabbit anti-human ACTH, Zymed Laboratories, San Francisco) and secondary (goat anti-rabbit IgG, 1:200 dilution, Vector Laboratories, Inc.) antisera and visualized by the chromogen DAB and counterstained with hematoxylin according to methods provided in the Vectastain ABC kit (Vector Laboratories, Inc.).

Bone marrow, lymph nodes, spleen, and thymus cells

Organs were obtained from wild-type or mutant animals and transferred to PBS supplemented with 2% calf serum. Single cell suspensions were prepared by squeezing organs between two frosted microscope slides in RPMI-1640 media with 10% FBS. Live cells (based on trypan blue exclusion) were counted on a hemocytometer. Thymus cellularity was determined from six wild-type and six p18-null (1-month-old) animals. Spleen cellularity was determined from four wild-type and four p18-null (2-month-old) animals. Bone marrow cellularity was determined from nine wild-type and nine p18-null (2-month-old) animals.

To analyze T-cell populations, cells obtained from the thymus, lymph nodes, and spleen were stained with FITC-conjugated rat monoclonal antibody to mouse CD4 and phycoerythrin (PE)-conjugated rat antibody to mouse CD8 (Caltag Laboratories). Splenic and bone marrow B cell populations were measured by staining with FITC-conjugated goat antibody to mouse IgM and PE-conjugated rat antibody to mouse CD45R (B220; Caltag). Nonviable cells were excluded by propidium iodide (PI) staining and cell scatter profile. All FACS analyses were carried out from a total of six wild-type and six p18-null animals by use of the FACSCAN flow cytometer (Becton-Dickinson) and Cyclops 2000 version 4 data analysis software (Cytomation).

For in vitro stimulation, 5×10^5 lymph node cells from 4-week-old mice were cultured in 200 µl of RPMI-1640 medium supplemented with 10% FBS, with or without 5 µg/ml ConA (Sigma) in 96-well flat-bottom plates. After 54 hr, [^{3}H]thymidine (1 µCi per well, NEN) was added, and cells were cultured for an additional 18 hr. Labeled cells were harvested, and incorporated ^{3}H was measured by a liquid scintillation counter. The experiment was performed using triplicate cultures from three wild-type and three p18-mutant animals. To stimulate lymphocytes in vivo, mice were injected intraperitoneally with 100 µg ConA in 0.3 ml of sterile PBS. After 12 hr, mice were sacrificed, lymph nodes were harvested and single cell suspensions were prepared. Immediately, 8×10^5 cells were incubated with [^{3}H]thymidine in 96-well plates (1 µCi per well) for 12 hr at 37°C in RPMI-1640 supplemented with 10% FBS. The labeled cells were harvested, and incorporated ^{3}H was measured. The experiment was repeated twice with triplicate cultures from two wild-type and two p18-null animals.

High density resting B lymphocytes isolated from the spleen of 2-month-old wild-type or p18-null mice by Percoll gradient centrifugation were cocultured (4.5×10^5 cells/p60 dish at a density of 1.5×10^5 cells/ml) with mitotically arrested L cells expressing the mouse CD40L. In separate cultures, the B lymphocytes were co-cultured with L cells expressing mouse CD40L in the presence of recombinant IL-6 (40 U/ml) synthesized in baculovirus as described previously (Morse et al. 1997). The soluble IL-6 receptor gp80 synthesized in baculovirus (40 U/ml) was also added to enhance the formation of the high-affinity IL-6 receptor. The biological activity of IL-6 and soluble gp80 was determined by induction of B-lymphocyte terminal differentiation in CESS cells (Morse et al. 1997). Viable cells were counted after trypan blue staining every 24 hr for 6 days. The experiment was repeated three times with triplicate cultures from two wild-type and two p18-null animals.

Apoptosis assay

Three wild-type and three p18-null (4-week-old) mice were used for the in vivo T-lymphocyte apoptosis assays. Two wild-type and two p18-null animals were injected intraperitoneally with dexamethasone for 12 hr (0.5 mg of dexamethasone in 0.3 ml of sterile PBS). One wild-type animal and one p18-null animal were injected with 0.3 ml of sterile PBS as mock controls. Mouse thymocytes were harvested as described above. Apoptotic cells were assayed by terminal deoxynucleotide transferase (TdT) end labeling analysis as described previously (Su et al. 1995). Resting B-lymphocyte populations were purified from four wild-type and four p18-null animals and cultured in duplicate in the presence of CD40L with or without IL-6 as detailed

above. At each time point, cells were analyzed for early apoptotic cells with FITC-conjugated annexin V antibody and PI double staining according to methods provided in the Apoptosis Detection kit (Oncogene Research Products, Inc., Cambridge, MA).

Acknowledgments

We are particularly grateful to Dr. Beverly Koller for her advice and technical support in generating targeted ES cell lines, karyotypic analysis, and blastocyst microinjection. We thank Dr. Andrew Koff for providing p27 mutant mice and Dr. Michael Schell for helping with the statistical analysis. We also thank Drs. Deborah O'Brien, Bob Duronio, Terry van Dyke, and Dawn Phelps for discussion and reading of the manuscript. D.S.F. is a recipient of National Research Service Awards from the National Institutes of Health/National Institute of Arthritis and Musculoskeletal and Skin Diseases (NIH/NIAMS). L.S. is a Basil O'Connor Scholar and a recipient of a R.J. Reynolds Award. Y.X. is a Pew Scholar in Biomedical Science and recipient of an American Cancer Society Junior Faculty award. This study was supported by a NIH grants AR43455 and AR44580 to S.C-K., CA65572 and CA68377 to Y.X.

The publication costs of this article were defrayed in part by payment of page charges. This article must therefore be hereby marked 'advertisement' in accordance with 18 USC section 1734 solely to indicate this fact.

References

Deng, C., P. Zhang, J.W. Harper, S.J. Elledge, and P. Leder. 1995. Mice lacking $p21^{CIP1/WAF1}$ undergo normal development, but are defective in G1 checkpoint control. *Cell* **82:** 675–684.

Fero, M.L., M. Rivkin, M. Tasch, P. Porter, C.E. Carow, E. Firpo, K. Polyak, L.-H. Tsai, V. Broudy, R.M. Perlmutter, K. Kaushansky, and J.M. Roberts. 1996. A syndrome of multiorgan hyperplasia with features of gigantism, tumorigenesis, and female sterility in $p27^{Kip1}$-deficient mice. *Cell* **85:** 733–744.

Franklin, D.S. and Y. Xiong. 1996. Induction of $p18^{INK4c}$ and its predominant association with CDK4 and CDK6 during myogenic differentiation. *Mol. Biol. Cell* **7:** 1587–1599.

Guan, K.-L., C.W. Jenkins, Y. Li, M.A. Nichols, X. Wu, C.L. O'Keefe, A.G. Matera, and Y. Xiong. 1994. Growth suppression by p18, a $p16^{INK4/MTS1}$- and $p14^{INK4B/MTS2}$-related CDK6 inhibitor, correlates with wild-type pRb function. *Genes & Dev.* **8:** 2939–2952.

Hu, N., A. Gutsmann, D.C. Herbert, A. Bradley, W.-H. Lee, and E.Y.-H.P. Lee. 1994. Heterzygous *Rb*-1^{D20}/+ mice are predisposed to tumors of the pituitary gland with a nearly complete penetrance. *Oncogene* **9:** 1021–1027.

Hunter, T. and J. Pines. 1994. Cyclins and cancer II: Cyclin D and CDK inhibitors come of age. *Cell* **79:** 573–582.

Jacks, T., A. Fazeli, E.M. Schmitt, R.T. Bronson, M.A. Goodell, and R.A. Weinberg. 1992. Effects of an Rb mutation in the mouse. *Nature* **359:** 295–300.

Jenkins, C.W. and Y. Xiong. 1995. Immunoprecipitation and immunoblotting in cell cycle studies. In *Cell cycle: Material and methods*. (ed. M. Pagano) pp. 250–263. Springer-Verlag, New York, NY.

Kiyokawa, H., R.D. Kineman, K.O. Manova-Todorova, V.C. Soares, E.S. Hoffman, M. Ono, D. Khanam, A.C. Hayday, L.A. Frohman, and A. Koff. 1996. Enhanced growth of mice lacking the cyclin-dependent kinase inhibitor function of $p27^{Kip1}$. *Cell* **85:** 721–732.

Lee, Y.-H.P., C.-Y. Chang, N. Hu, Y.-C.J. Wang, C.-C. Lai, K. Herrup, W.-H. Lee, and A. Bradley. 1992. Mice deficient for Rb are nonviable and show defects in neurogenesis and haematopoiesis. *Nature* **359:** 288–294.

Mathews, L.S., R.E. Hammer, R.R. Behringer, A.J. D'Ercole, G.I. Bell, R.L. Brinster, and R.D. Palmiter. 1988. Growth enhancement of transgenic mice expressing human insulin-like growth factor I. *Endocrinol.* **123:** 2827–2833.

Meyerson, M. and E. Harlow. 1994. Identification of G1 kinase activity for cdk6, a novel cyclin D partner. *Mol. Cell. Biol.* **14:** 2077–2086.

Morgan, D.O. 1995. Principles of CDK regulation. *Nature* **374:** 131–134.

Morse, L., D. Chen, D.S. Franklin, Y. Xiong, and S. Chen-Kiang. 1997. Induction of cell cycle arrest and B cell terminal differentiation by CDK inhibitor $p18^{INK4c}$ and IL-6. *Immunity* **6:** 47–56.

Nakayama, K., N. Ishida, M. Shirane, A. Inomata, T. Inoue, N. Shishido, I. Horii, D.Y. Loh, and K.-I. Nakayama. 1996. Mice lacking $p27^{Kip1}$ display increased body size, multiple organ hyperplasia, retinal dysplasia, and pituitary tumors. *Cell* **85:** 707–720.

Palmiter, R.D., R.L. Brinster, R.E. Hammer, M.E. Trumbauer, M.G. Rosenfeld, N.C. Birnberg, and R.M. Evans. 1982. Dramatic growth of mice that develop from eggs microinjected with metallothionein-growth hormone fusion genes. *Nature* **300:** 611–615.

Pardee, A.B. 1989. G1 events and regulation of cell proliferation. *Science* **246:** 603–608.

Phelps, D. and Y. Xiong. 1997. Assay for cyclin D-dependent kinases 4 and 6. *Methods Enzymol.* **283:** 194–205.

———. 1998. Regulation of CDK4 during adipogenesis involves switching of cyclin D subunits and concurrent binding of $p18^{INK4c}$ and $p27^{KIP1}$. *Cell Growth. Differ.* **9:** 595–610.

Phelps, D., K.-M. Hsiao, Y. Li, N. Hu, D.S. Franklin, E. Westphal, E.Y.-H.P. Lee, and Y. Xiong. 1998. Coupled transcriptional and translational control of the CDK inhibitor $p18^{INK4c}$'s expression during myogenesis. *Mol. Cell. Biol.* **18:** 2334–2343.

Quaife, C.J., L.S. Mathews, C.A. Pinkert, R.E. Hammer, R.L. Brinster, and R.D. Palmiter. 1989. Histopathology associated with elevated levels of growth hormone and insulin-like growth factor I in transgenic mice. *Endocrinol.* **124:** 40–48.

Reynisdottir, I. and J. Massague. 1997. The subcellular locations of $p15^{Ink4b}$ and $p27^{Kip1}$ coordinate their inhibitory interactions with cdk4 and cdk2. *Genes & Dev.* **11:** 492–503.

Reynisdottir, I., K. Polyak, A. Iavarone, and J. Massague. 1995. Kip/Cip and Ink4 Cdk inhibitors cooperate to induce cell cycle arrest in response to TGF-β. *Genes & Dev.* **9:** 1831–1845.

Robanus Maandag, E.C., M. Van Der Valk, M. Vlaar, C. Feltkamp, J. O'Brien, M. Van Roon, N. Van Der Lugt, A. Berns, and H. Te Riele. 1994. Developmental rescue of an embryonic-lethal mutation in the retinoblastoma gene in chimeric mice. *EMBO J.* **13:** 4260–4268.

Serrano, M., H.-W. Lee, L. Chin, C. Cordon-Cardos, D. Beach, and R.A. DePinho. 1996. Role of the INK4a locus in tumor suppression and cell mortality. *Cell* **85:** 27–37.

Sherr, C.J. 1994. G1 phase progression: Cycling on cue. *Cell* **79:** 551–555.

———. 1996. Cancer cell cycle. *Science* **274:** 1672–1677.

Sherr, C.J. and J.M. Roberts. 1995. Inhibitors of mammalian G_1 cyclin-dependent kinases. *Genes & Dev.* **9:** 1149–1163.

Su, L., H. Kaneshima, M. Bonyhadi, S. Salimi, D. Kraft, L. Rabin, and J.M. McCune. 1995. HIV-1 induced thymocyte depletion is associated with indirect cytopathicity and infection of progenitor cells in vivo. *Immunity* **2:** 25–36.

Tybulewicz, V.L.J., C.E. Crawford, P.K. Jackson, R.T. Bronson, and R.C. Mulligan. 1991. Neonatal lethality and lymphopenia in mice with a homozygous disruption of the c-*abl* proto-oncogene. *Cell* **65:** 1153–1163.

Van Kooten, C. and J. Banchereau. 1997. Function of CD40 on B cells, dendritic cells and other cells. *Curr. Opin. Immunol.* **9:** 330–337.

Williams, B.O., E.M. Schmitt, L. Remington, R.T. Bronson, D.M. Albert, R.A. Weinberg, and T. Jacks. 1994. Extensive contribution of Rb-deficient cells to adult chimeric mice with limited histopathological consequences. *EMBO J.* **13:** 4251–4259.

Xiong, Y., H. Zhang, and D. Beach. 1993. Subunit rearrangement of cyclin-dependent kinases is associated with cellular transformation. *Genes & Dev.* **7:** 1572–1583.

Yan, Y., J. Frisen, M.-H. Lee, J. Massague, and M. Barbacid. 1997. Ablation of the CDK inhibitor $p57^{Kip2}$ results in increased apoptosis and delayed differentiation during mouse development. *Genes & Dev.* **11:** 973–983.

Yang, R., A.F. Gombart, M. Serrano, and H.P. Koeffler. 1995. Mutational effects of the $p16^{INK4a}$ tumor suppressor protein. *Cancer Res.* **55:** 2503–2506.

Zhang, P., N. Liegeois, C. Wong, M. Finegold, H. Hou, J.C. Thompson, A. Silverman, J.W. Harper, R.A. DePinho, and S.J. Elledge. 1997. Altered cell differentiation and proliferation in mice lacking $p57^{KIP2}$ indicates a role in Beckwith-Wiedemann syndrome. *Nature* **387:** 151–158.

Zindy, F., H. Soares, K.-H. Herzog, J. Morgan, C.J. Sherr, and M.F. Roussel. 1997. Expression of INK4 inhibitor of cyclin D-dependent kinases during brain development. *Cell Growth Differ.* **8:** 1139–1150.